NATIONAL RESEARCH COUNCIL OF CANADA
CONSEIL NATIONAL DE RECHERCHES DU CANADA

NATIONAL AERONAUTICAL ESTABLISHMENT

LABORATORY TECHNICAL REPORT

LTR - UA - 19

EXPERIMENTAL DAMPING - IN - PITCH OF TWO SLENDER CONES AT MACH 2 AND INCIDENCES UP TO 30°

S. IYENGAR

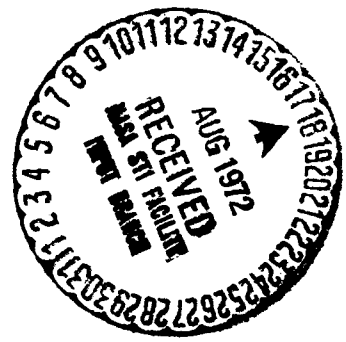

RAPPORT TECHNIQUE DE LABORATOIRE

ÉTABLISSEMENT AÉRONAUTIQUE NATIONAL

JANUARY 1972

OTTAWA, CANADA

NATIONAL AERONAUTICAL ESTABLISHMENT

ÉTABLISSEMENT AÉRONAUTIQUE NATIONAL

CANADA

PAGES 17

FIG. DIAG. 8

REPORT RAPPORT

REPORT RAPPORT LTR-UA-19

DATE January 1972

SECTION

UNSTEADY AERODYNAMICS

LAB. ORDER COMM. LAB. N.A.E. 752

FILE DOSSIER M49-10N-5

FOR POUR Partially supported by the National Aeronautics and Space Administration, U.S.A., under contract NASW-1947

REFERENCE RÉFÉRENCE

LTR- UA-19

EXPERIMENTAL DAMPING-IN-PITCH OF TWO SLENDER CONES AT MACH 2 AND INCIDENCES UP TO 30°

SUBMITTED BY PRÉSENTÉ PAR K. Orlik-Rückemann
SECTION HEAD
CHEF DE SECTION

AUTHOR AUTEUR S. Iyengar

APPROVED APPROUVÉ F.R. Thurston
DIRECTOR
DIRECTEUR

FORM NRC 538
FORMULAIRE NRC 538

COPY NO. 3
COPIE NR.

ABSTRACT

Oscillatory experiments were performed on two slender cones at Mach 2 and incidences up to 30°, using three different experimental arrangements. The damping-in-pitch was found to remain constant at incidences of up to a value approximately corresponding to the cone semi-angle, after which an almost linear increase with incidence was noted. The results obtained with the different techniques were in very good agreement up to an incidence of 15° and in some cases up to 25°.

TABLE OF CONTENTS

1 INTRODUCTION

Very little information is available at present on the hypersonic damping-in-pitch of bodies of revolution at non-zero incidence. This report describes an investigation in the N.A.E. 30 in. x 16 in. suction wind tunnel where this quantity was determined for two slender right circular cones at a Mach number of 2 and at incidences of up to 30°. Since the character of the model boundary layer could be expected to affect the damping-in-pitch results, all the experiments were performed with and without boundary layer trip near the nose of the model.

Although oscillatory experiments on circular cones can be performed most conveniently using the standard technique of full-models with internal excitation, two additional experimental techniques were also employed for evaluation purposes. This comprised the full-model technique with external excitation, which was originally developed for experiments on flat and slender configurations (such as elliptical cones), and the half-model technique, which has recently found wide application for testing multi-body configurations (such as the shuttle spacecraft), configurations that lack a rear centerbody suitable for sting mounting (such as F14, F15) and configurations with simulated jet exhaust plume. The report presents a comparison of the damping-in-pitch results obtained with all these experimental techniques in order to assess the potential applicability of the two above mentioned special techniques to experiments involving non-zero incidences. This comparison is further supported by surface flow visualization photographs obtained for both half-models and full-models at various incidences.

The part of the investigation dealing with the determination of stability derivatives using the standard technique of full-model with internal excitation was partially supported by the National Aeronautics and Space Administration of the United States under contract NASW-1947. All the remaining parts were carried out as part of the internal research programme of the National Aeronautical Establishment. For completeness all the results are presented in this single report, regardless of their origin.

2 WIND TUNNEL

All the tests were performed in the N.A.E. 30 in. x 16 in. supersonic air tunnel. This is an intermittent suction tunnel with run times of 12-14 secs. Interchangeable nozzle liners are used to obtain discrete Mach numbers in the range 1.2 to 2.0. The tests presented here were done at a Mach number of 2.0. Tunnel stagnation pressure was about 1 atmosphere and intake air was dried to a specific humidity not exceeding 0.0005. The Reynolds number per foot was approximately 3.6×10^6.

3 EXPERIMENTAL TECHNIQUES

3.1 Full-Model with Internal Excitation

The full-model was sting-mounted with the main stiffness of the oscillatory system being provided by a cantilever spring (Fig. 1A). This spring was attached to an adapter at the front and anchored to the sting at the rear via a flexible link. The model was fixed to the adapter by means of two screws. The adapter was connected to the

sting through a flexural pivot that defined the center of oscillation of the model. Figure 1B shows the adapter (left centre), the cantilever spring with flexible link attached (right centre) and the flexural pivot (below adapter).

Model oscillation was produced by a solenoid-actuated tripper. The tripper is shown mounted on top of the sting in Fig. 1B (bottom). The motion of the solenoid was transmitted to the tripper via an actuator rod (top of Fig. 1B). This rod passed through a narrow guideway drilled inside the sting. The actuator was made up of two parts, one of which varied in length to accommodate the varying strut boss lengths (for different incidences). The different struts used are shown in Fig. 1D. The tripper was spring-loaded so that it could only pivot forward; it made contact with a replaceable metal pad screwed to the rear of the model.

The cantilever spring was strain gauged and calibrated to obtain a direct relation between the model angular deflection and the strain-gauge output.

The solenoid required about 70 to 90 volts to oscillate the model. Once the tripper was inside the model, a voltage of 30 to 40 volts was sufficient to keep it inside until the model oscillation had reached its lower bound. At this point, the power to the solenoid was turned off so that the tripper came out of the model after which the voltage level was again increased to about 80 volts and power turned on to oscillate the model once more. This cycle of operations was repeated as many times as necessary. A variac was used to provide the variable voltage to the solenoid.

Figure 1C shows details of the model-sting-tripper assembly. Figure 1E illustrates the model mounted on the 30° strut. At the lower right-hand corner one can see the solenoid with its spring-loaded plunger.

3.2 Full-Model with External Excitation

This technique is described in detail in Ref. 1. The model was sting-mounted from the rear and attached to the sting by means of miniature frictionless flexural pivots. The main stiffness of the oscillatory system was provided by a pair of gimbal springs mounted outside the tunnel on the top and bottom walls, respectively, and attached (through another flexural pivot) to the base of the model by pre-stressed piano wires. These wires were shielded from the flow by wedge-shaped wire guards. One of the springs was electro-magnetically-driven, providing oscillatory motion to the system. The motion of the other spring was recorded by a linear variable displacement transducer whose output was therefore proportional to the model deflection.

Three stings were used for this method - a rectangular cross-section sting (similar to the one shown at the bottom of Fig. 2 but without the tripper), a circular cross-section sting (top of Fig. 2) and a bent sting of rectangular cross-section (middle of Fig. 2). Four struts holding the sting were used, one each for incidences of 0°, 10°, 20°, and 30°. The bent sting with a bend of 5° was used to obtain incidences of 5°, 15° and 25°. The four struts and the base (to which they were attached by 2 screws) are shown in Fig. 1D.

3.3 Half-Model

Details of model mounting are given in Refs 2 and 3. Briefly, the half-model was elastically mounted in an electromechanical oscillator. The model was located outside the tunnel wall boundary layer and separated by a narrow gap of the order of 0.01 in., from a reflection plate that was mounted parallel to the wall at a distance of about 0.5 in. Small end plates (fences) were mounted at the inside surface of the models (i.e. at what would have been the virtual symmetry plane of the full-model) to minimize gap effects.

3.4 Test Procedures and Data Reduction

In all the methods employed, the free oscillation technique was used. For the full-model technique with external excitation and for the half-model technique the standard method of the "free oscillation with automatically recycled feedback excitation" was used (Ref. 2). For the full-model technique with internal excitation each collapse was individually triggered. Before a run, tare damping and frequency at ambient pressure were obtained from the Dampometer by driving the model out to an amplitude of 2° (or deflecting it in the internally-driven case) and letting it collapse (10 times in all). Tare damping and frequency in vacuum (or at a known low pressure) were also measured. The tunnel was then run and as many collapses as possible were obtained before the flow break-down (which was monitored by a pressure transducer on the tunnel floor). To ensure that mechanical conditions were the same before and after the run, tare damping and frequency were measured once more immediately after the run.

Tests were performed at nominal mean incidences of 0°, 5°, 10°, 15°, 20°, 25°, and 30°. The single mean amplitude of oscillation used was 1.5°. In all cases the actual mean incidence (i.e. the equilibrium incidence around which the model oscillated due to a finite aerodynamic pitching moment) did not differ by more that 0.3° from the nominal value.

During the tests, the linearity of the system was checked frequently (at least during one run for each condition) by monitoring the output of the model position transducer on a recording oscillograph and subsequently plotting the model amplitude versus time on a semi-logarithmic graph.

Model base pressure and test section pitot and static pressures were measured with pressure transducers located outside the tunnel. For every run the test section static pressure was monitored on one channel of a recording oscillograph to ensure that the flow was constant for the duration of the damping measurement.

Run duration was of the order of 13 to 14 secs, allowing, on the average, three to four damping cycles per run.

3.4.1 Data Reduction

The expressions for static and dynamic pitching moment derivatives are (Ref. 3),

$$C_{m\theta} = \frac{\partial C_m}{\partial \theta} = \frac{2M_\theta}{\rho V^2 S \ell} = \frac{-8\pi^2 I(\nu^2 - \nu_0{}^2)}{\rho V^2 S \ell} \qquad (1)$$

$$C_{m\dot{\theta}} = \frac{\partial C_m}{\partial \left(\frac{\ell\dot{\theta}}{2V}\right)} = \frac{4M_{\dot{\theta}}}{\rho V S \ell^2} = \frac{-8I}{\rho V S \ell^2}\left[\delta\nu - \frac{\delta_0\nu_0}{2}\left(1+\frac{\nu_0}{\nu}\right)\right] \qquad (2)$$

where $C_m = \dfrac{M}{1/2\ \rho V^2 S \ell}$

M = pitching moment

$1/2\ \rho V^2$ = free-stream dynamic pressure

S = base area of model

ℓ = model length

I = moment of inertia of oscillating system

$\theta, \dot{\theta}$ = angle of oscillation in pitch about a fixed axis and its first derivative with respect to time

δ = logarithmic decrement

ν = oscillation frequency, Hz

$()_0$ = conditions at zero pressure

The terms in the square bracket of Eq. (2) indicate that the damping was assumed to be viscous and hysteretic in equal proportions. The logarithmic decrement and frequency were obtained from the paper tape of the Dampometer.

3.4.2 Correction for Sting Oscillation

With the full-model techniques (both internal and external excitation) the effect of sting oscillation had to be accounted for and usually resulted in a rearward shift in the positions of the effective axis of oscillation. Details of this correction are given in Appendix I.

4 MODELS

The circular cone of semi-vertex angle 7.75° was geometrically similar to one of the models of Ref. 4 and was also tested in the N.A.E. helium hypersonic wind tunnel (Ref. 5). It had a nominal length of 9 in. A semi-vertex angle of 10° was chosen for the other cone since coning motion experiments on a 10° semi-vertex angle cone at incidence were being conducted at the NASA Ames Research Center (Ref. 6) and the two sets of results were directly relevant. Both full-models were hollow while the half-models were solid. The surface of all models (steel) was hand polished. Figure 3 shows the two full-models (left) and the two half-models, one with a fence and the other with an adapter.

5 EXPERIMENTAL PROGRAMME

The four models - two half and two full - were tested at mean incidences from 0° to 30° inclusive, in increments of 5°. All three techniques were used for the entire range of incidences. Furthermore, for each model and incidence, tests were performed with and without a 0.02 in. thick nylon boundary layer trip glued to the model about 0.50 in. from the tip.

Axis positions for the cones were chosen in such a way that the static margin always remained small and positive. This ensured that the equilibrium mean incidence around which the models oscillated was within a fraction of a degree of the nominal mean incidence. A larger departure from the nominal value could otherwise cause the models to hit the mechanical stop which was incorporated in the system and completely prevent the oscillation. Nominal axis positions of $x_0/\ell=0.61$ for the 10° cone and $x_0/\ell=0.65$ for the 7.75° cone were chosen.

The frequency of oscillation for the different models was between 30 - 45 Hz, corresponding to a reduced frequency ($\omega\ell/2V$) range of 0.041 to 0.069.

6 RESULTS

The results obtained herein are presented in Figs 4 to 7, along with the zero incidence first - and second - order potential theory (Ref. 7). Figures 4 and 5 show the variation of the dynamic and static stability derivatives with mean incidence. It is to be noted that because of sting oscillation the position of the axis of oscillation is different for the various techniques. Figures 6 and 7 show the variation of $\alpha C_{m\dot{\theta}}$ with α. In these figures $C_{m\dot{\theta}}$ has been "normalized" with respect to the axis position for the full-model with internal excitation, using the following axis-transfer equation (Ref. 8),

$$C_{m\dot{\theta}_2} = C_{m\dot{\theta}_1} - \frac{x}{\ell} C_{N\dot{\theta}_1} + \frac{2x}{\ell} C_{m\theta_1}\cos\alpha - 2\left(\frac{x}{\ell}\right)^2 C_{N\theta}\cos\alpha + 4\,\frac{x}{\ell} C_{m_1}\sin\alpha - 4\left(\frac{x}{\ell}\right)^2 C_N\sin\alpha$$

where subscript '1' refers to the aft axis and subscript '2' to the parallel forward axis at a distance x upstream, and in which

C_m = pitching moment coefficient

C_N = normal force coefficient

α = mean incidence

Since all the aerodynamic coefficients and derivatives on the right hand side are based on zero incidence theory (Ref. 7), the normalization is valid, strictly speaking, only for low incidence cases. However, for the sake of uniformity, it has been applied to the entire range of incidence covered by the experiments.

It was felt that of the three methods employed, the full-model with internal excitation would probably be the most reliable. It was reasoned that, since the mechanical system was internal to the model, this method would create the least interference effects. It is for this reason that in both Figs 6 and 7 the data obtained from each of the other techniques are compared with the data obtained using the full-model with internal excitation. Only damping derivatives were considered in these figures since they were of primary concern for this investigation.

7 DISCUSSION

7.1 Effect of Boundary Layer Trip

For the 7.75° cone at zero incidence (Figs 4A and 4B) the boundary layer trip had a large effect on the damping derivative as measured by the two full-model techniques. At all other incidences the results with and

without the trip were in good agreement. The half-model data were unaffected by the presence of the trip (Fig. 4C)

Figure 4A also shows an almost linear variation of $C_{m\dot{\theta}}$ with incidence for mean incidences greater that 15°. Figures 4A and 4B show the good agreement between the theory of Ref. 7 and the zero incidence experimental data using a trip. The half-model data are also in good agreement with the theory at $\alpha=0$ (Fig. 4C). All figures indicate an increasing static stability up to $\alpha=20°$ and a subsequent destabilizing effect.

The effect of the trip on the damping derivative at zero incidence is much less pronounced for the 10° cone (Figs 5A and 5B). The damping derivative is relatively constant up to $\alpha=10°$ and gradually increases for greater incidences. The agreement at $\alpha=0$ with the theory is good for all three methods (Figs 5A, 5B & 5C).

The large effect on damping of the boundary layer trip for the 7.75° cone at $\alpha=0°$ (and a smaller effect for the 10° cone) cannot be fully explained at present. It is possible that an effect similar to that reported in Ref. 9 may be responsible. It was suggested in that reference that in cases when boundary layer transition occurs near the base on a flat-based cone, a plunging sting may create a high enough adverse pressure in the base area to move the transition upstream thereby increasing the damping. No experiments were undertaken to determine whether transition actually took place near the base. A calculation of the Reynolds number based on cone length, however, did indicate a strong possibility of transition occuring near the base, especially for the

7.75° cone.

Tests carried out at higher frequencies (100 Hz) produced greater sting oscillation and an even higher $C_{m\dot{\theta}}$ for the 7.75° cone at $\alpha=0$ without a trip (results not presented here). The corresponging effect on the 10° cone was less. All this would seem to add certain credibility to the possibility of dynamic sting interference being responsible for the large damping increase at zero incidence without the trip.

In this connection, the average model base pressure was measured and was found to be fairly constant (ratio of base pressure to tunnel static pressure $\simeq$ 0.35) with or without the trip.

7.2 Effect of Incidence

As stated earlier, one of the primary purposes of this investigation was to obtain damping data at high incidences on circular cones. On both full-models, damping remained fairly constant up to an incidence of 10° (Figs 4A, 4B, 5A, 5B). At higher incidence, in the internal excitation case damping increased almost linearly with incidence.[+] This rate of increase was smaller for the 10° cone than for the 7.75° cone (Figs 4A, 5A). The full-model with external excitation also displayed an increase in damping at incidences higher than 10°, the increase being not quite linear (Figs 4B, 5B). The half-model data for the 7.75° cone showed an almost linear variation of damping with mean incidence over the range of incidences investigated (Fig. 4C) while for the 10° cone damping was almost constant over the entire range (Fig. 5C).

[+]Added in proof: These results are in very good agreement with both the experimental and the theoretical results recently published in Ref. 11.

7.3 Comparison of the Two Full-Model Techniques

Figures 6A and 7A show a good agreement between the two techniques up to $\alpha=25°$. At $\alpha=30°$ the data obtained with the full-model (external excitation) technique are considerably lower. It is suspected that this effect may be due to the interference of the wire guards (used with external excitation) and the flow near the base of the model.

7.4 Comparison of Half-Model and Full-Model with Internal Excitation

Figure 6B shows very good agreement between the two methods for the 7.75° cone up to a mean incidence of 20°. For the 10° cone agreement is excellent up to $\alpha=15°$ (Fig. 7B) and fairly good at $\alpha=20°$. At higher incidences the half-model is less damped. At such high incidences the leeward flow field is known to contain two relatively unstable vortices. The presence of the reflection plate is likely to affect the position of the vortex sheet and thus produce a different flow field (with possibly different pressure distributions) around the half-model. At lower incidences the flow fields are likely to be similar. Preliminary results of a surface oil flow visualization experiment (Ref. 10) appear to confirm this hypothesis as demonstrated on Fig. 8 which shows the surface flow on the leeward side of the 10° cone at an incidence of 20°. The meridional position of the primary separation line on the full-model and on the half-model was the same within better than one degree[+], even if the corresponding positions of the secondary separation line differed by as much as five degrees (the separation line was closer to the leeward meridian on the full-model). At an incidence of 30° much more distinct differences in the flow patterns over the two models could be observed.

[+]The effect of boundary layer trip was negligible.

7.5 Comparison with other Results

As pointed out earlier, one of the major reasons for including the 10° cone in the present series of experiments was that it was hoped to compare damping-in-pitch results with results obtained from coning motion experiments (on a similar model and at the same Mach number) that were being conducted at NASA Ames Research Center (Ref. 6). It is pointed out in Ref. 6 that within a theoretical linear analysis the side moment coefficient resulting from pure coning motion should equal the quantity $\alpha C_{m\dot{\theta}}$ obtained from the damping-in-pitch experiments. Experimental measurements of the side moment coefficient were found to be in excellent agreement with the theoretical predictions of $\alpha C_{m\dot{\theta}}$ (Ref. 7) up to a mean incidence of 10°. The present experimental damping-in-pitch derivatives (using all three techniques) also exhibit a very good agreement of $\alpha C_{m\dot{\theta}}$ with theory up to a mean incidence of 10° as seen from Figs 6A, 6B, 7A and 7B. Thus, the theoretically predicted equality between side moment coefficient (pure coning motion) and $\alpha C_{m\dot{\theta}}$ (damping-in-pitch) is confirmed experimentally.

8 CONCLUSIONS

Within the range of experimental conditions investigated the following applies:

1. In the absence of boundary layer interference effects (such as may be associated with the probable boundary layer transition near the base on models without the boundary layer trip), the damping-in-pitch derivative of the two slender cones investigated remains constant for incidences approximately up to the cone semi-angle, after which it increases approximately linearly with incidence. This constant

value at low incidences is slightly higher than the prediction of supersonic potential theory.

2. The full-model technique with external excitation which was developed specially for testing flat models, gives satisfactory damping results for slender circular cones up to an incidence of 25°. At an incidence of 30° a considerable discrepancy with the results obtained with a standard full-model technique with internal excitation has been observed, which could have been caused by the interaction of wire guards with the flow in the model base area.

3. The half-model technique, which was developed specially for testing various unconventional and multi-body configurations, gives satisfactory damping results for slender circular cones up to an incidence of between 15° and 20°. At higher incidences a considerable discrepancy with the results obtained with a standard full-model technique with internal excitation has been observed, which could have been caused by the effect of the reflection plate and its associated boundary layer on the position of model leeside vortices. It may be expected that for wing-body configurations with a more stable vortex pattern than a circular cone, the half-model technique may yield satisfactory damping results also at higher incidences.

4. In connection with the results of Ref. 6 the results presented here offer experimental confirmation of a linear theoretical result that up to moderate incidences (~10°) the side moment coefficient measured from pure coning motion experiments is in good agreement with the quantity $\alpha C_{m\dot{\theta}}$ obtained from damping-in-pitch experiments.

9 ACKNOWLEDGEMENTS

The author is deeply indebted to Mr. L.T. Conlin, Mr. E. Peter and Mr. P. Pizzera for their invaluable assistance in designing, manufacturing the equipment and carrying out the experiments, respectively. He is also most grateful to Mr. J.G. LaBerge for many useful discussions.

10 REFERENCES

1. Orlik-Rückemann, K.J.
LaBerge, J.G.
Adams, P.A.
Conlin, L.T.
A Wind Tunnel Apparatus for Dynamic Stability Experiments on Sting Mounted Slender Bodies.
NRC NAE LTR-UA-13, March 1970.

2. Orlik-Rückemann, K.J.
Measurement of Aerodynamic Damping and Stiffness Derivatives in Free Oscillation with Automatically Recycled Feedback Excitation.
NRC NAE Aero Report LR-246, June 1959.

3. Orlik-Rückemann, K.J.
LaBerge, J.G.
Static and Dynamic Longitudinal Stability Characteristics of a Series of Delta and Sweptback Wings at Supersonic Speeds.
NRC NAE Aero Report LR-396, January 1966.

4. Jorgensen, L.H.
Elliptic Cones Alone and With Wings at Supersonic Speeds.
NACA Report 1376, 1958.

5. Orlik-Rückemann, K.J.
LaBerge, J.G.
Static and Dynamic Pitching Moment Measurements on a Family of Elliptic Cones at Mach Number 11 in Helium.
NRC NAE LTR-UA-14, July 1970.

6. Schiff, L.B.
Tobak, M.
Results from a New Wind Tunnel Apparatus for Studying Coning and Spinning Motions of Bodies of Revolution.
AIAA J. Vol. 8, No. 11, November 1970.

7. Tobak, M.
Wehrend, W.R.
Stability Derivatives of Cones at Supersonic Speeds.
NACA TN 3788, 1956.

8. Gilmore, A.
Seredinsky, V.
MacKenzie, D.
Investigation of Dynamic Stability Derivatives of Vehicles Flying at Hypersonic Velocity.
ASD-TDR-62-460, September 1963.

9. Ericsson, L.E.
Reding, J.P.
Boundary Layer Transition and Dynamic Sting Interference.
AIAA J. Vol. 8, No. 10, October 1970.

10. LaBerge, J.G.
Unpublished Results.

11. Stone, G.W.
Clark, Jr., E.L.
Burt, G.E.
An Investigation of Nonsymmetrical Aerodynamic Damping Moments.
AIAA 10th Aerospace Sciences Meeting, Paper no. 72-29, San Diego, January 1972.

APPENDIX I

In the following, the method used for calculating the shift in the location of the axis of oscillation due to sting vibration is described.

In the sketch below let δ_c be the deflection (relative to the wind) of the back of the model and δ_s the deflection of the sting at the location of the flexural pivot.

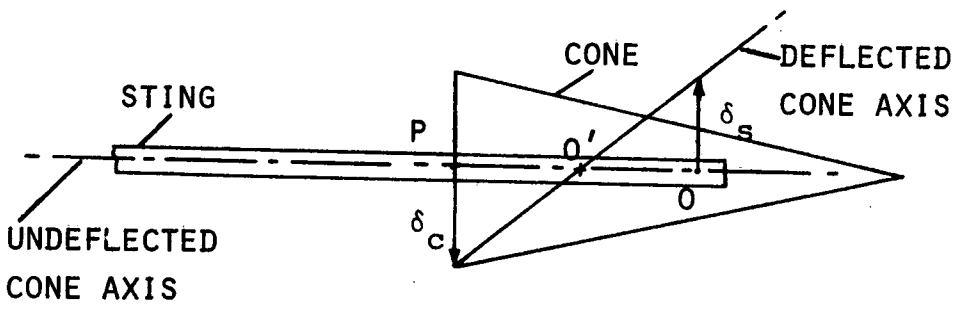

It is seen that if δ_s were = 0 (ideal case - no sting vibration) the cone would oscillate about point O. It was established, however, that the point O moved up when the cone nose moved up. For the instant under consideration, it is seen that the effective axis of oscillation is at position O' instead of O. The distance OO' is proportional to the ratio δ_s/δ_c and therefore the shift in axis location OO' would, in general, be a function of time: it was observed from an oscillograph trace, however, that the ratio of δ_s/δ_c was constant during a collapse. Therefore, the shift in axis location is constant. From the geometry of the figure,

$$\frac{OO'}{O'P} = \frac{\delta_s}{\delta_c}$$

$$\therefore \quad \frac{OO'}{(OP - OO')} = \frac{\delta_s}{\delta_c}$$

$$\text{and } OO' = \frac{OP \times \delta_s}{(\delta_c + \delta_s)}$$

The distance OP is known from the model geometry and δ_c and δ_s are measured.

The new axis location for the different cases is given below:

CONE	CASE	x_0/ℓ
7.75°	NOMINAL	0.65
	FULL-MODEL (EXTERNAL)	0.68
	FULL-MODEL (INTERNAL)	0.70
10°	NOMINAL	0.61
	FULL-MODEL (EXTERNAL)	0.63
	FULL-MODEL (INTERNAL)	0.65

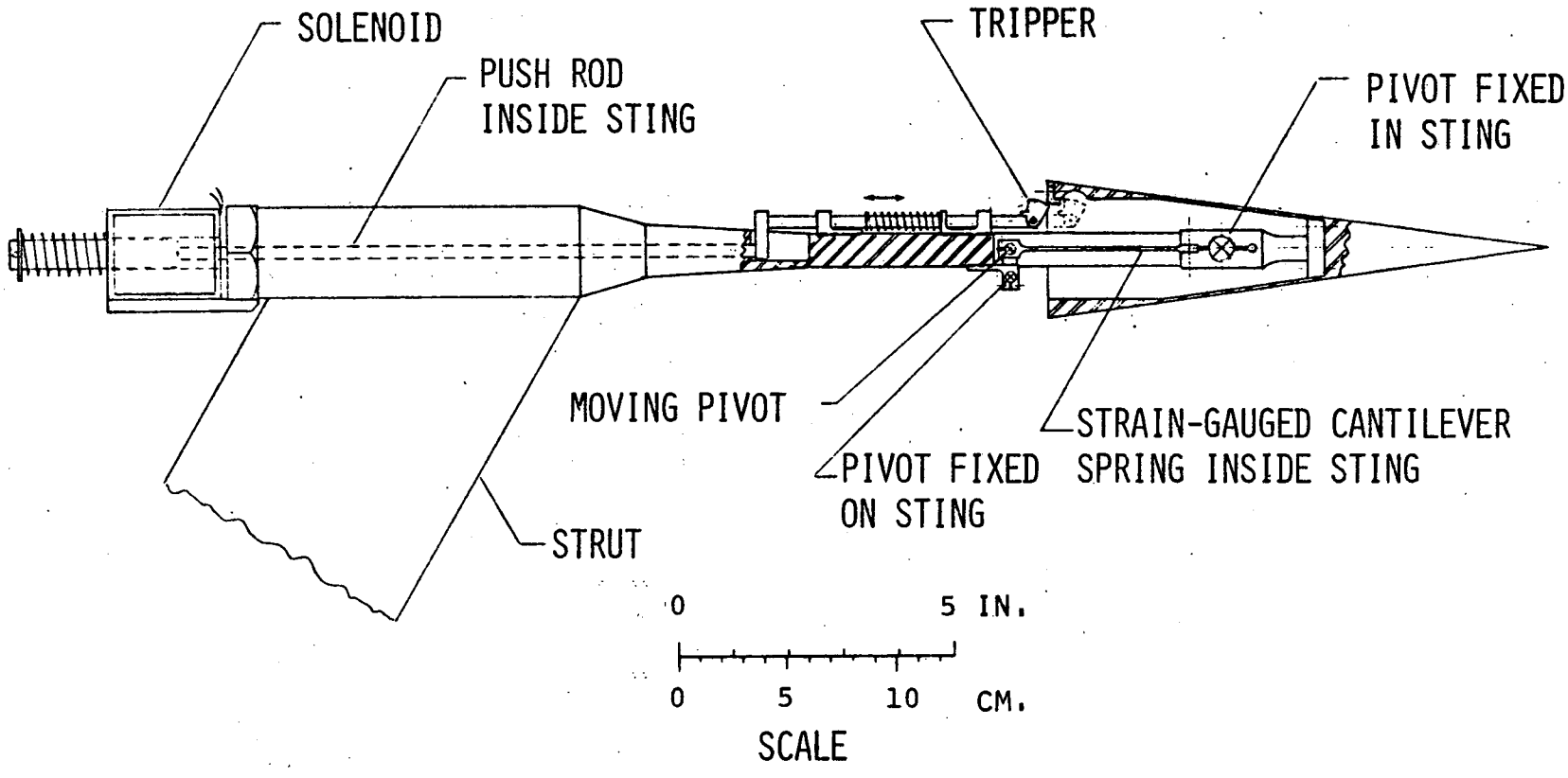

(A) SCHEMATIC

FIG. 1 EXPERIMENTAL ARRANGEMENT FOR FULL-MODEL WITH INTERNAL EXCITATION

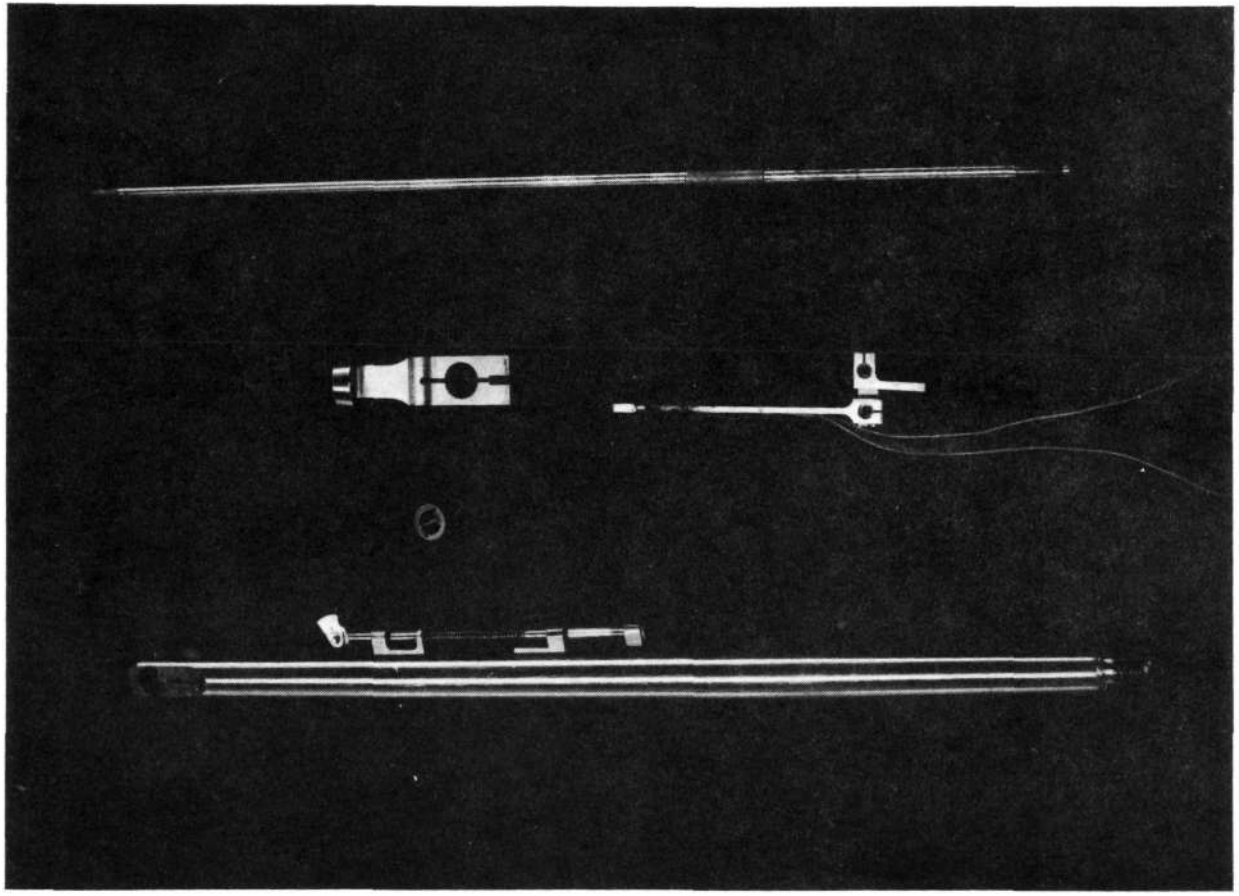

(B) DETAILS OF MODEL ATTACHMENT

FIG. 1 CONTINUED

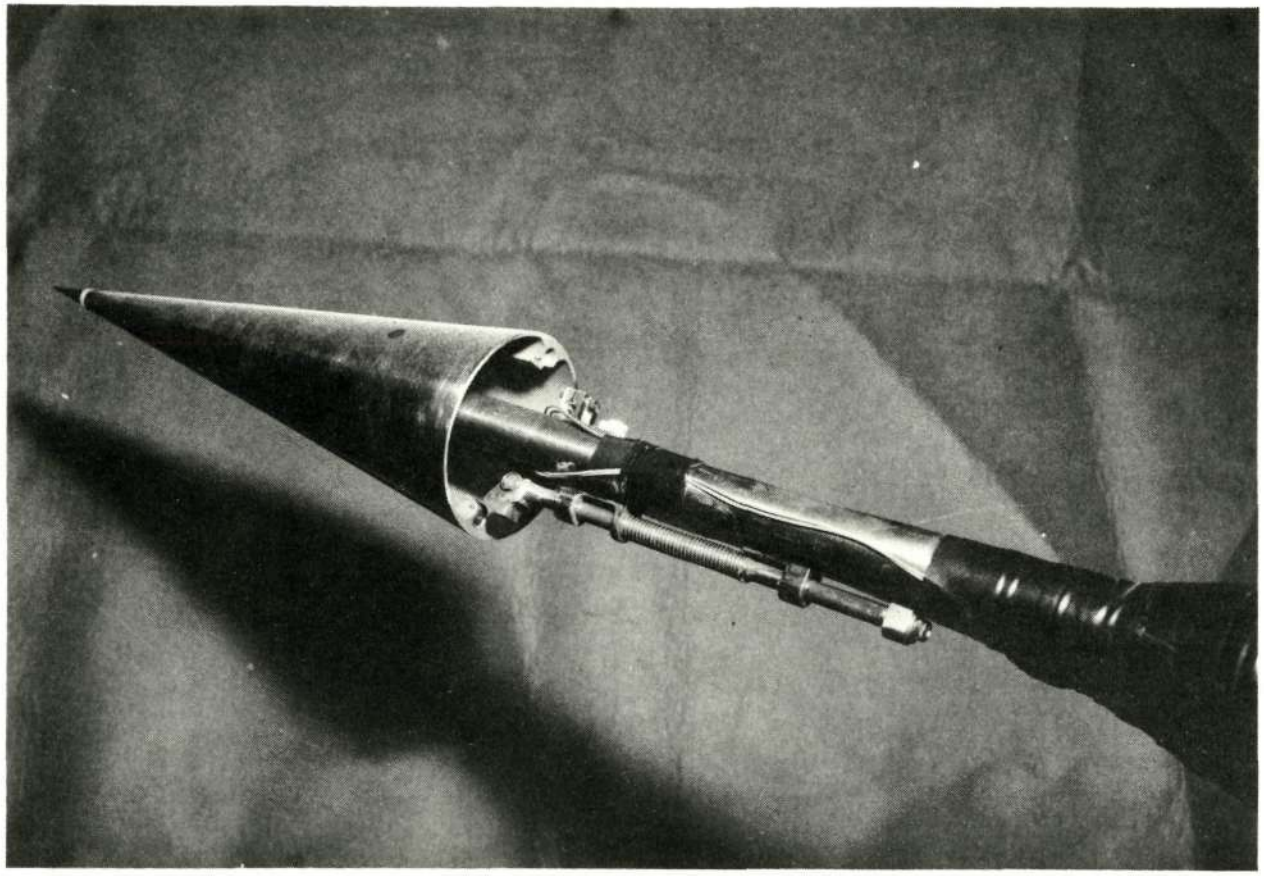

(c) ASSEMBLY OF MODEL EXCITATION MECHANISM

FIG. 1 CONTINUED

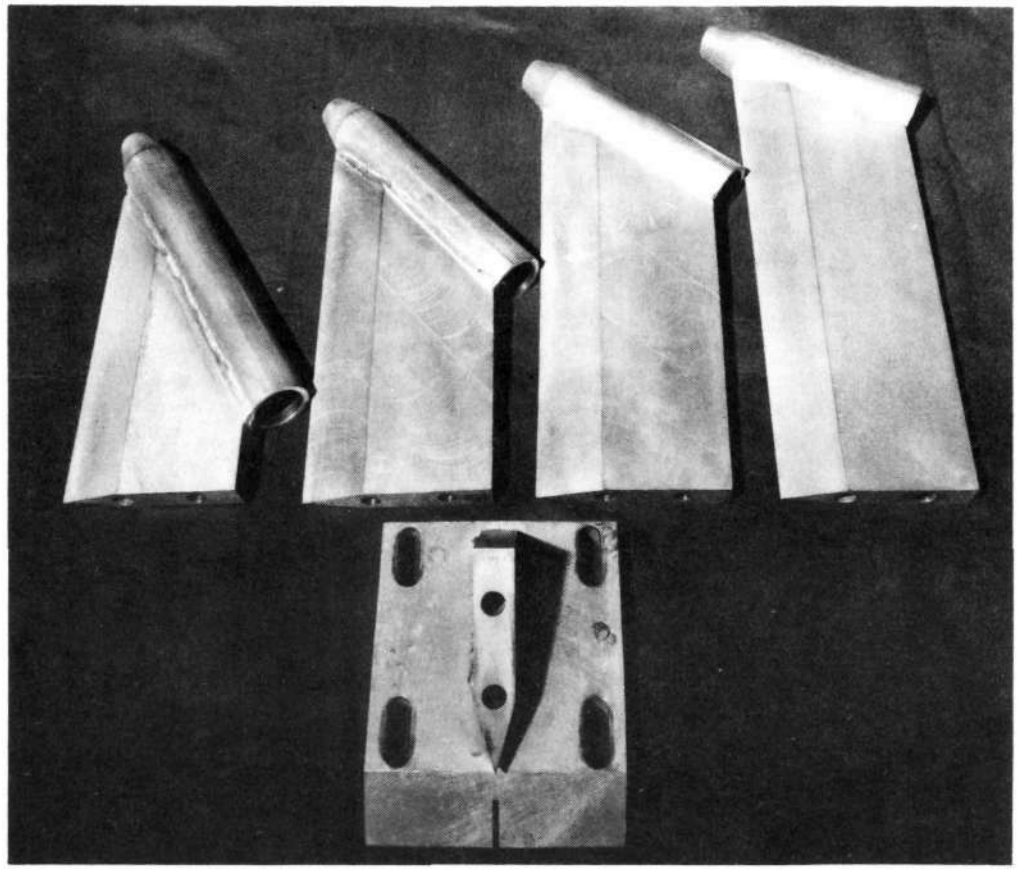

(D) STING SUPPORT STRUTS FOR VARIOUS INCIDENCES

FIG. 1 CONTINUED

(E) MODEL AND STING MOUNTED ON THE 30° STRUT

FIG. 1 CONCLUDED

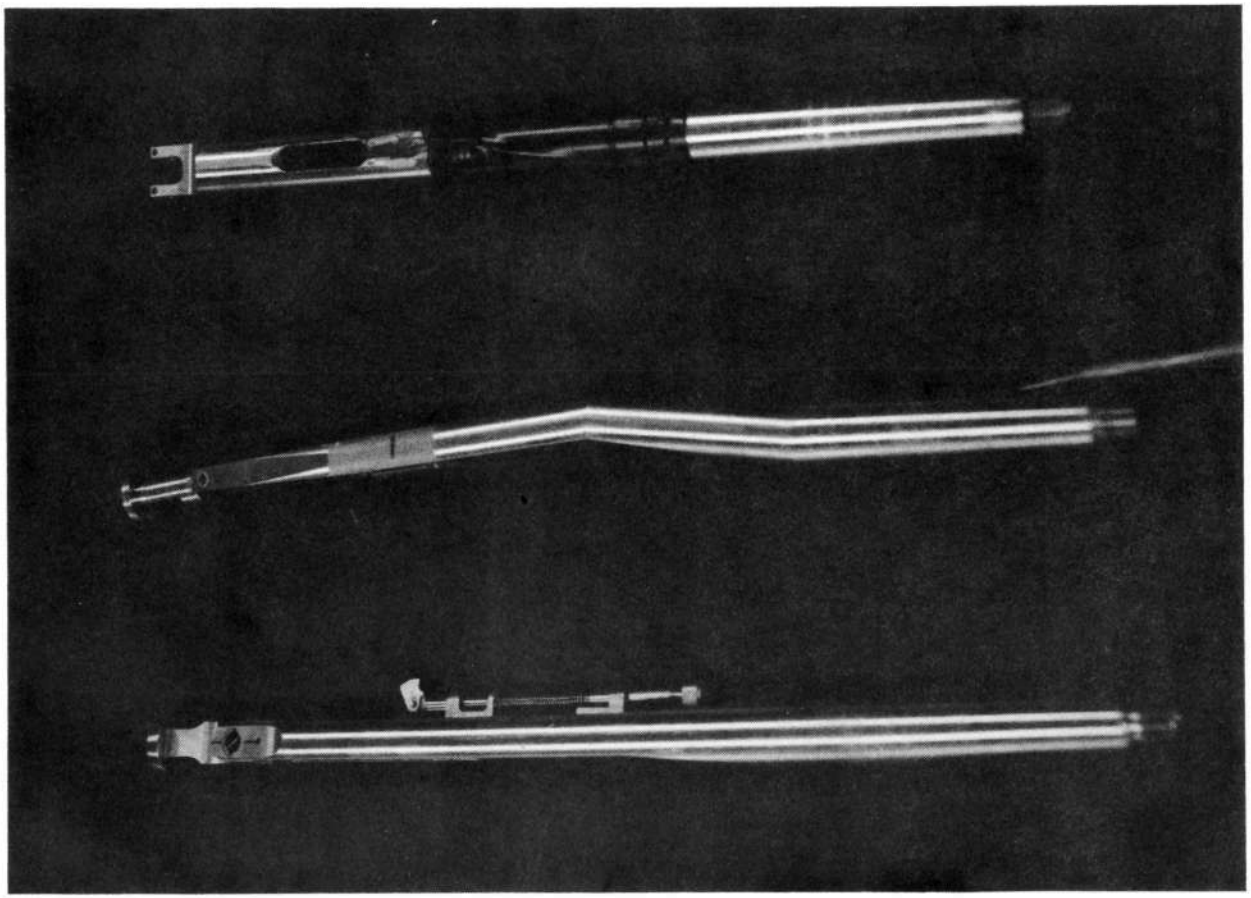

FIG. 2 STINGS USED FOR FULL-MODEL EXPERIMENTS

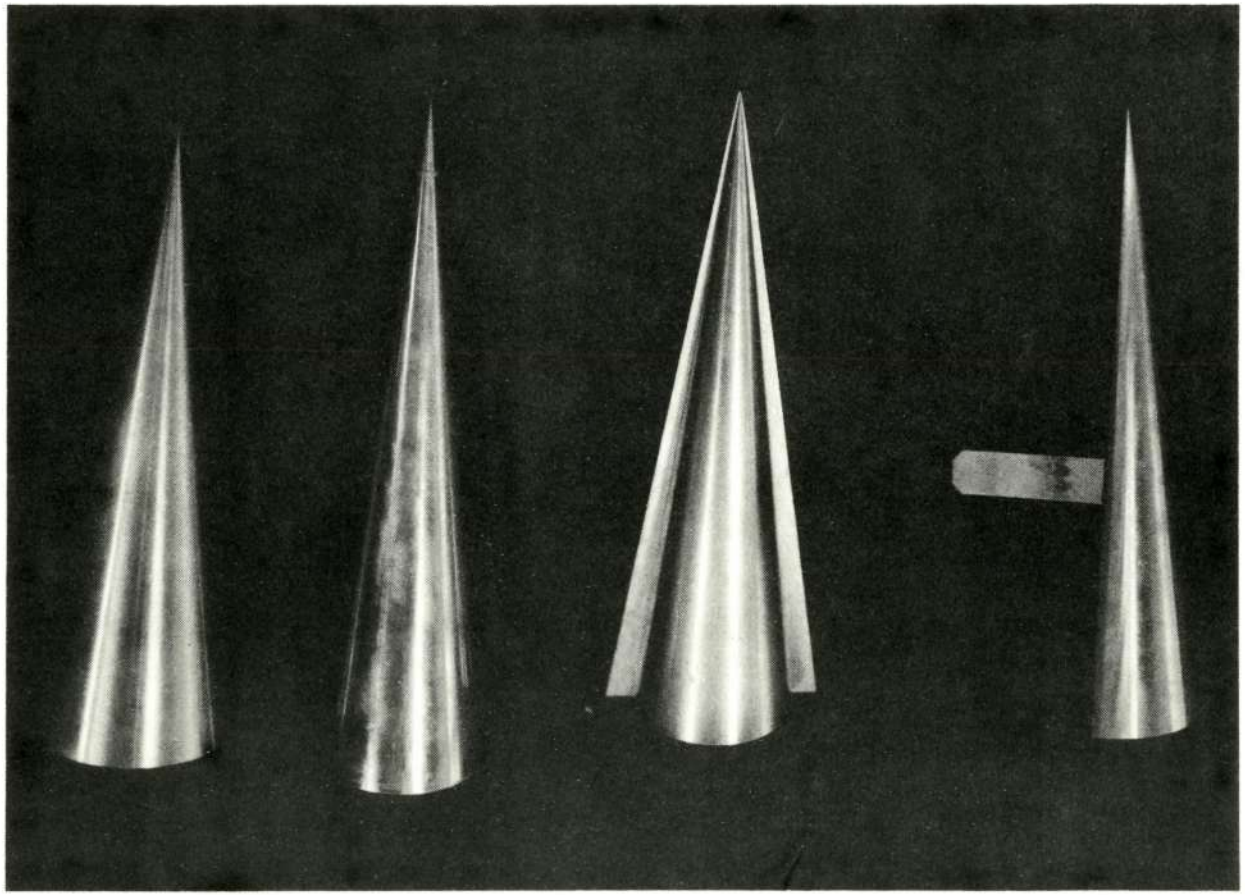

FIG. 3 FULL-MODELS AND HALF-MODELS USED IN THE INVESTIGATION.

FROM LEFT: 10° FULL-MODEL, 7.75° FULL-MODEL WITH TRIP,

7.75° HALF-MODEL WITH ROOT FENCE, 10° HALF-MODEL WITH ADAPTER.

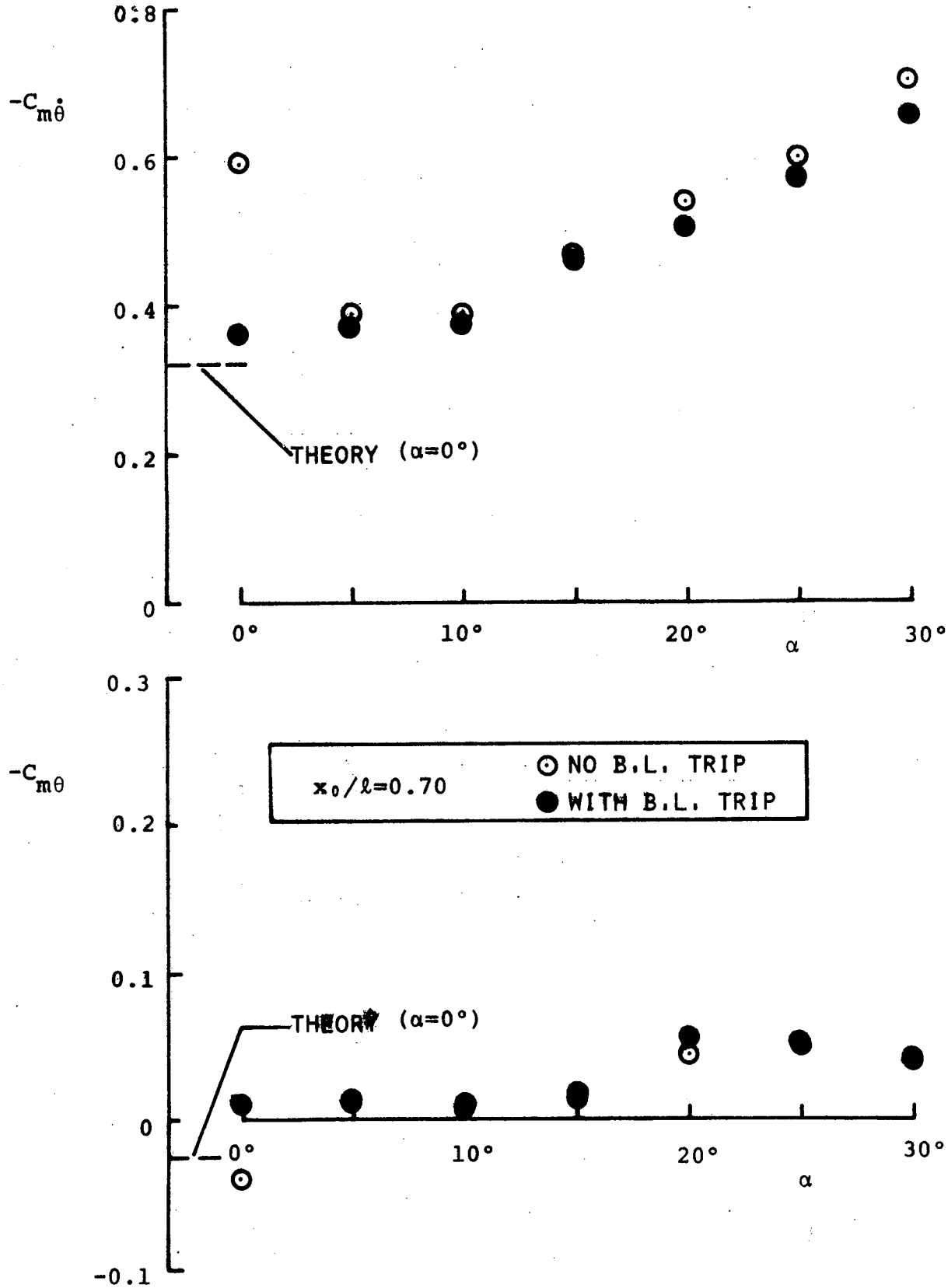

A) FULL-MODEL TECHNIQUE WITH INTERNAL EXCITATION

FIG. 4 EFFECT OF INCIDENCE ON STABILITY DERIVATIVES OF THE 7.75° CONE

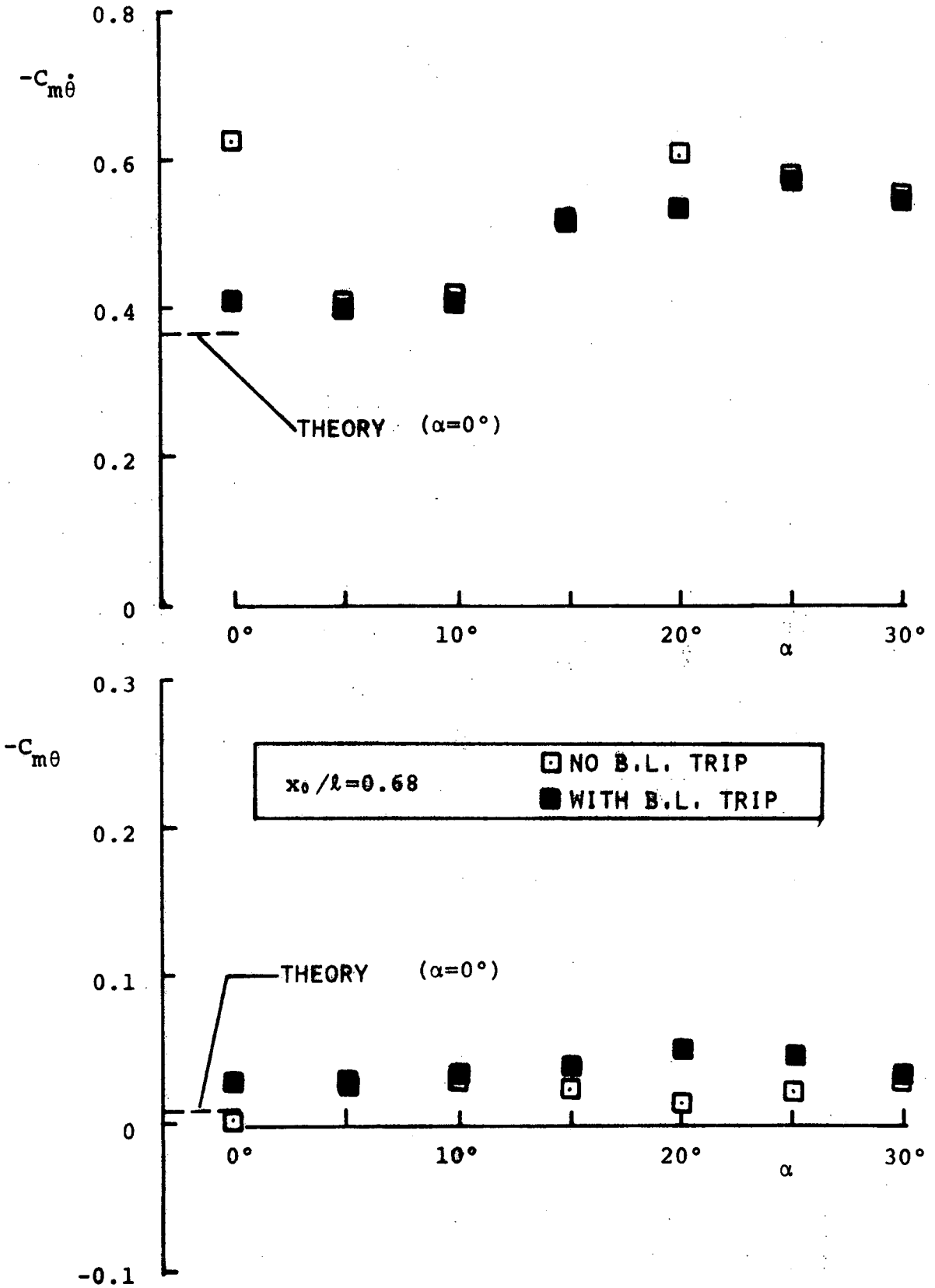

B) FULL-MODEL TECHNIQUE WITH EXTERNAL EXCITATION

FIG. 4 CONTINUED

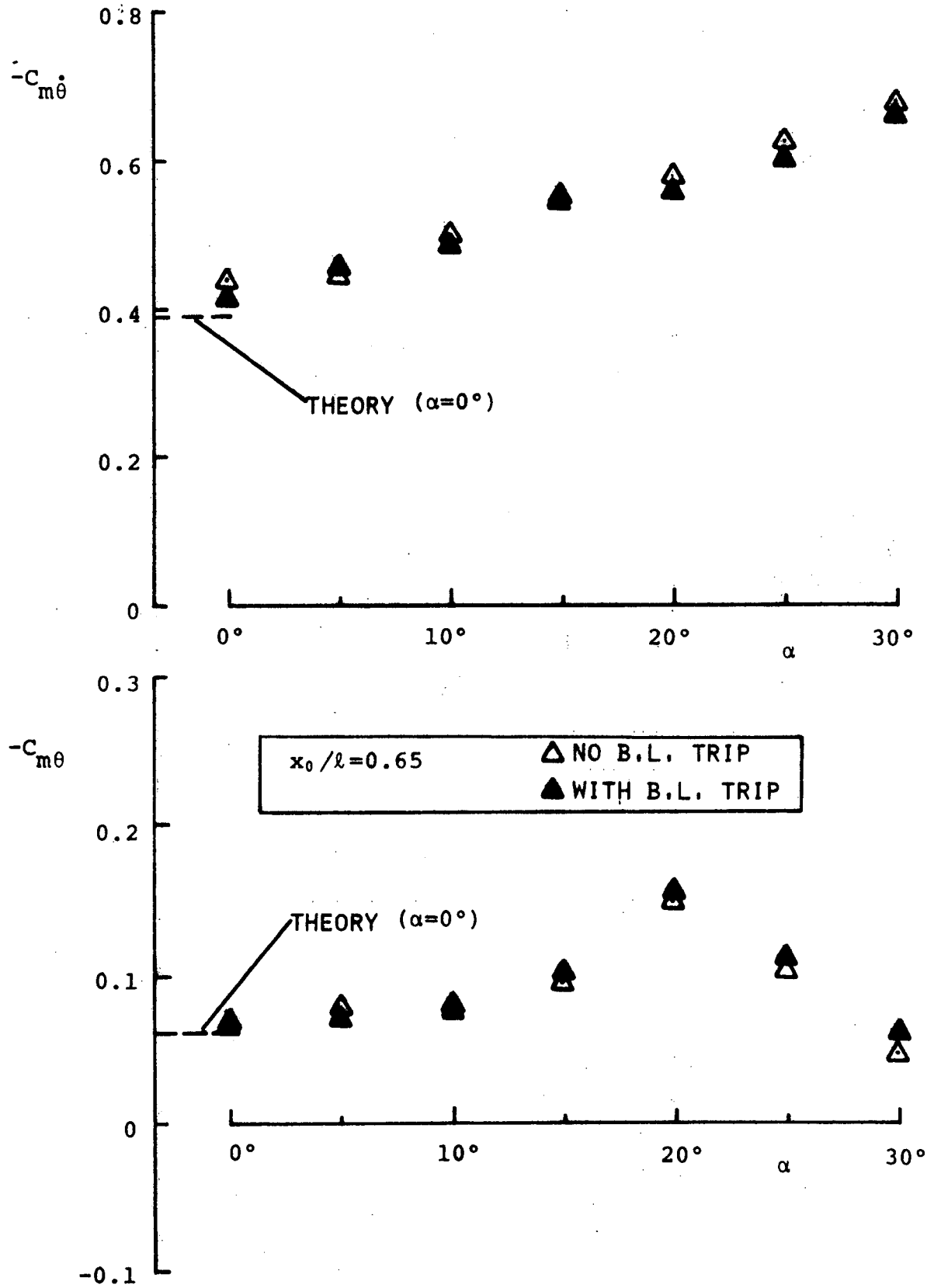

c) HALF-MODEL TECHNIQUE

FIG. 4 CONCLUDED

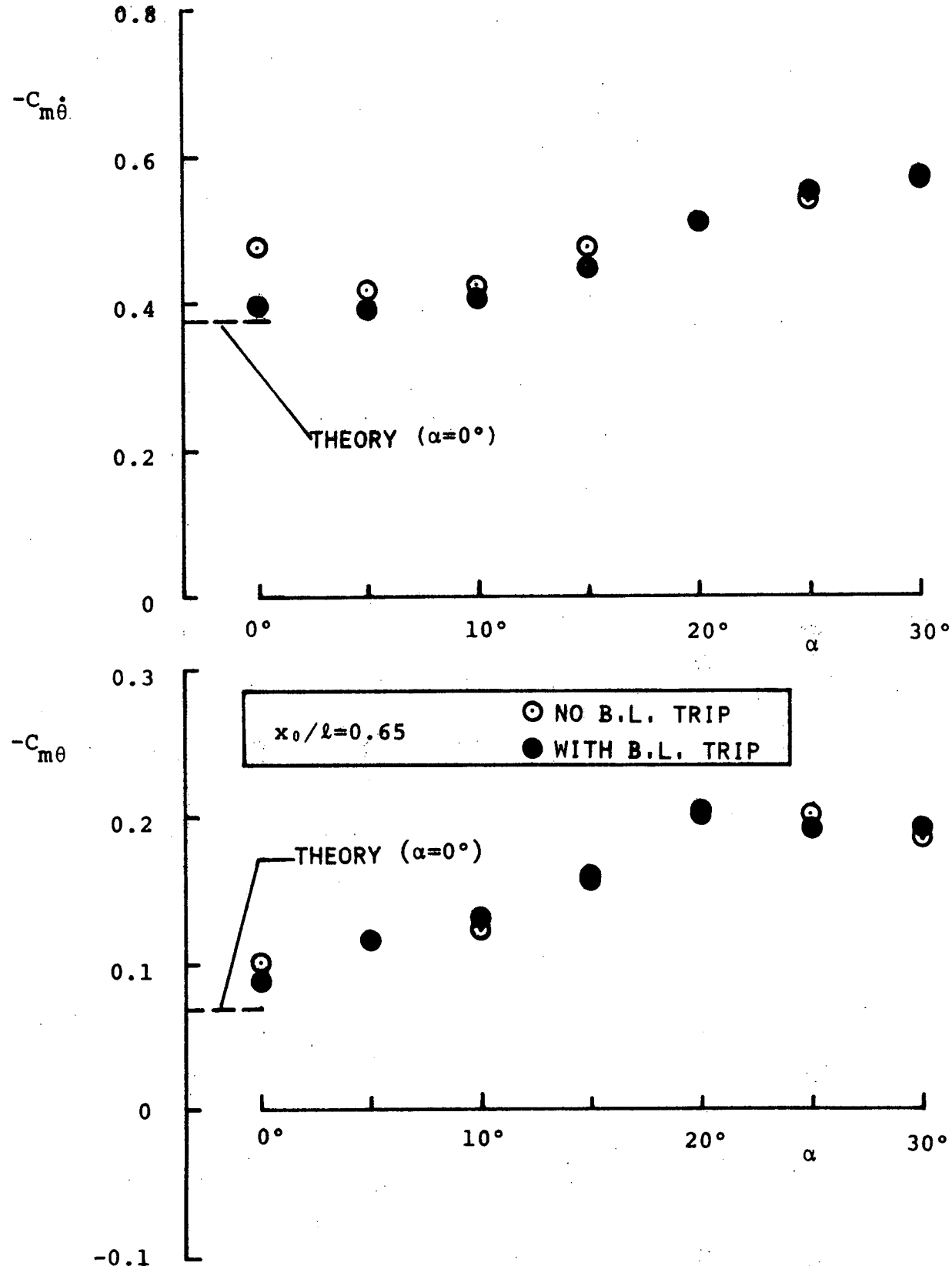

A) FULL-MODEL TECHNIQUE WITH INTERNAL EXCITATION

FIG. 5 EFFECT OF INCIDENCE ON STABILITY DERIVATIVES OF THE 10° CONE

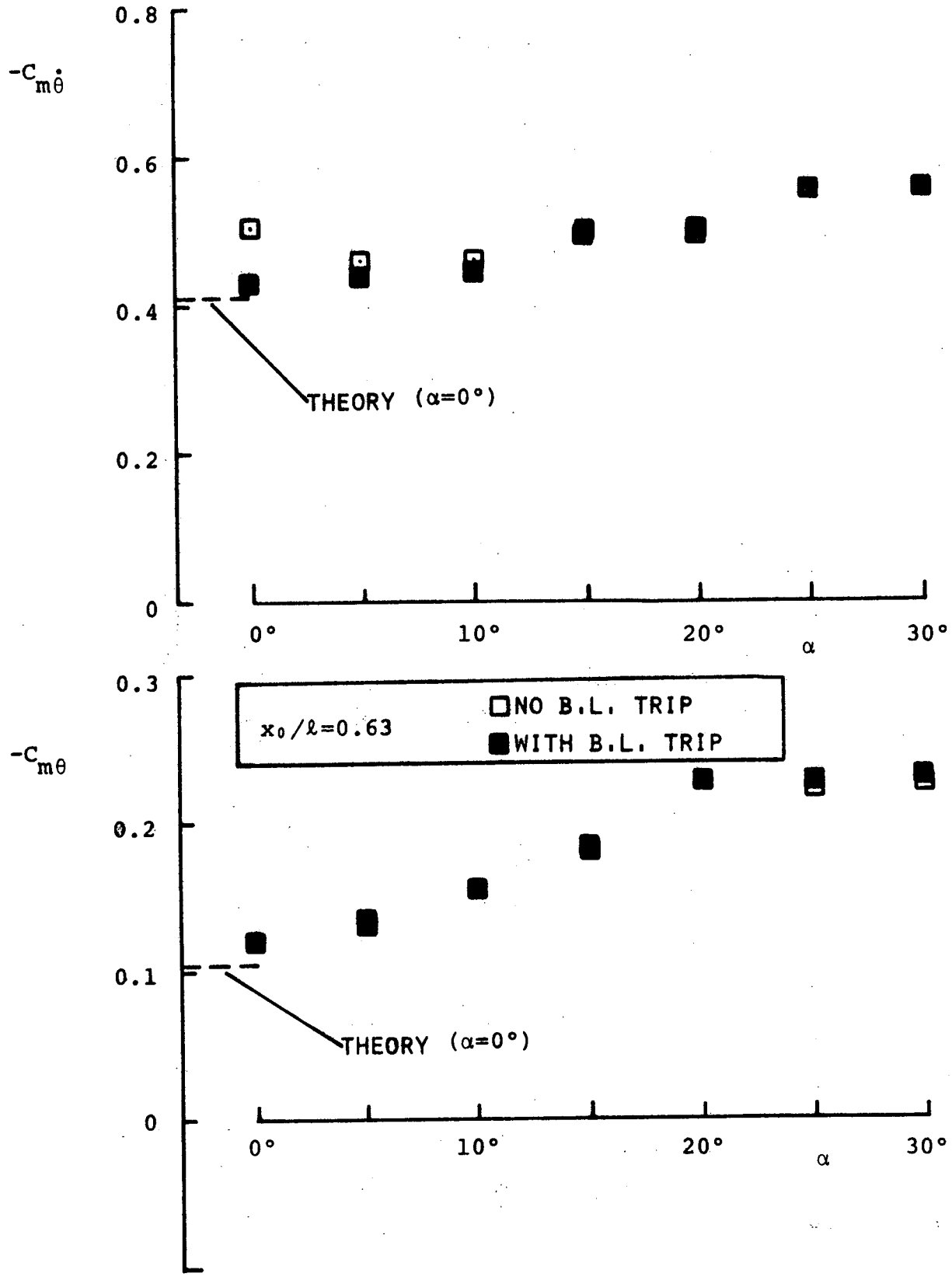

B) FULL-MODEL TECHNIQUE WITH EXTERNAL EXCITATION

FIG. 5 CONTINUED

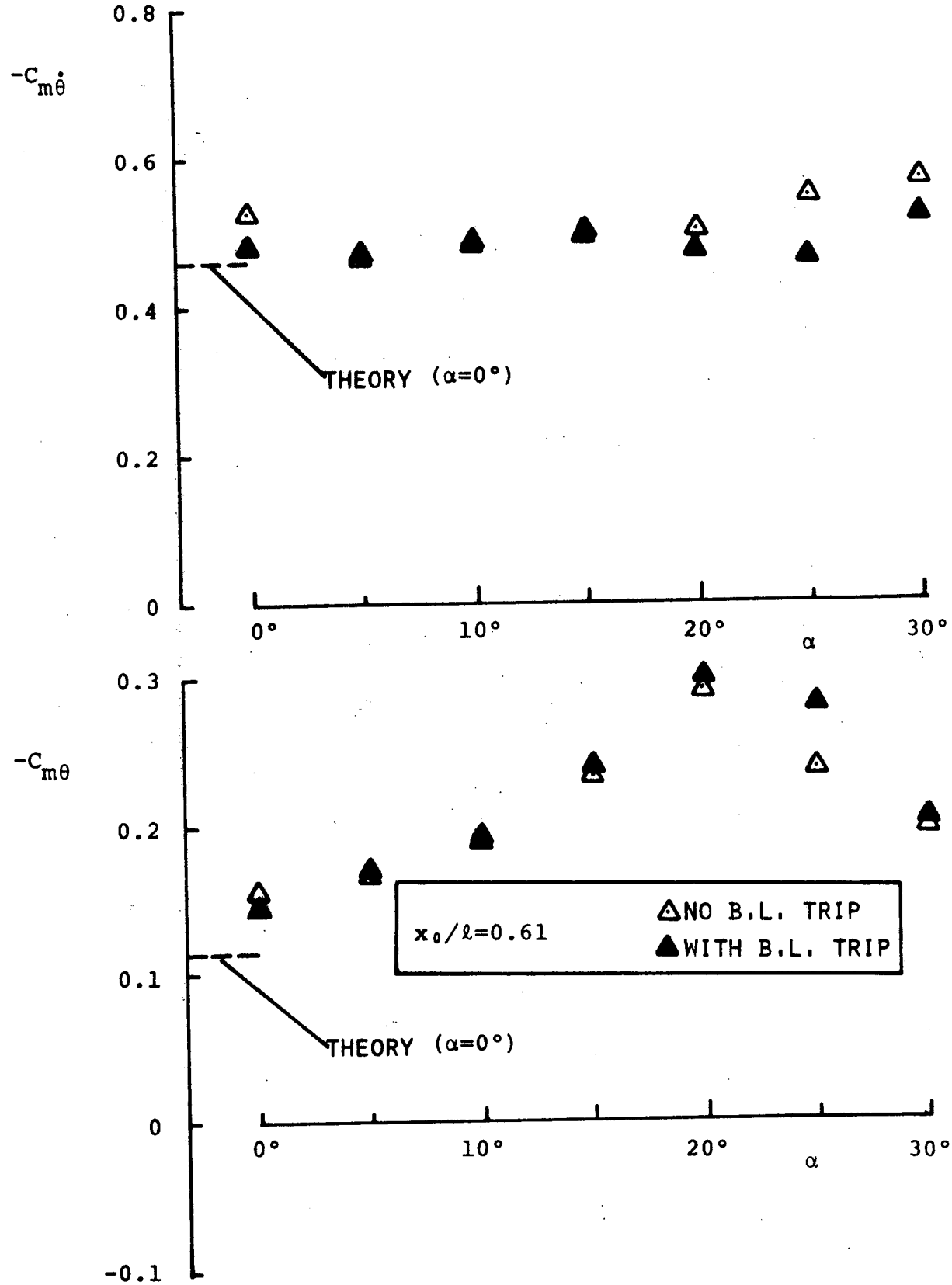

c) HALF-MODEL TECHNIQUE

FIG. 5 CONCLUDED

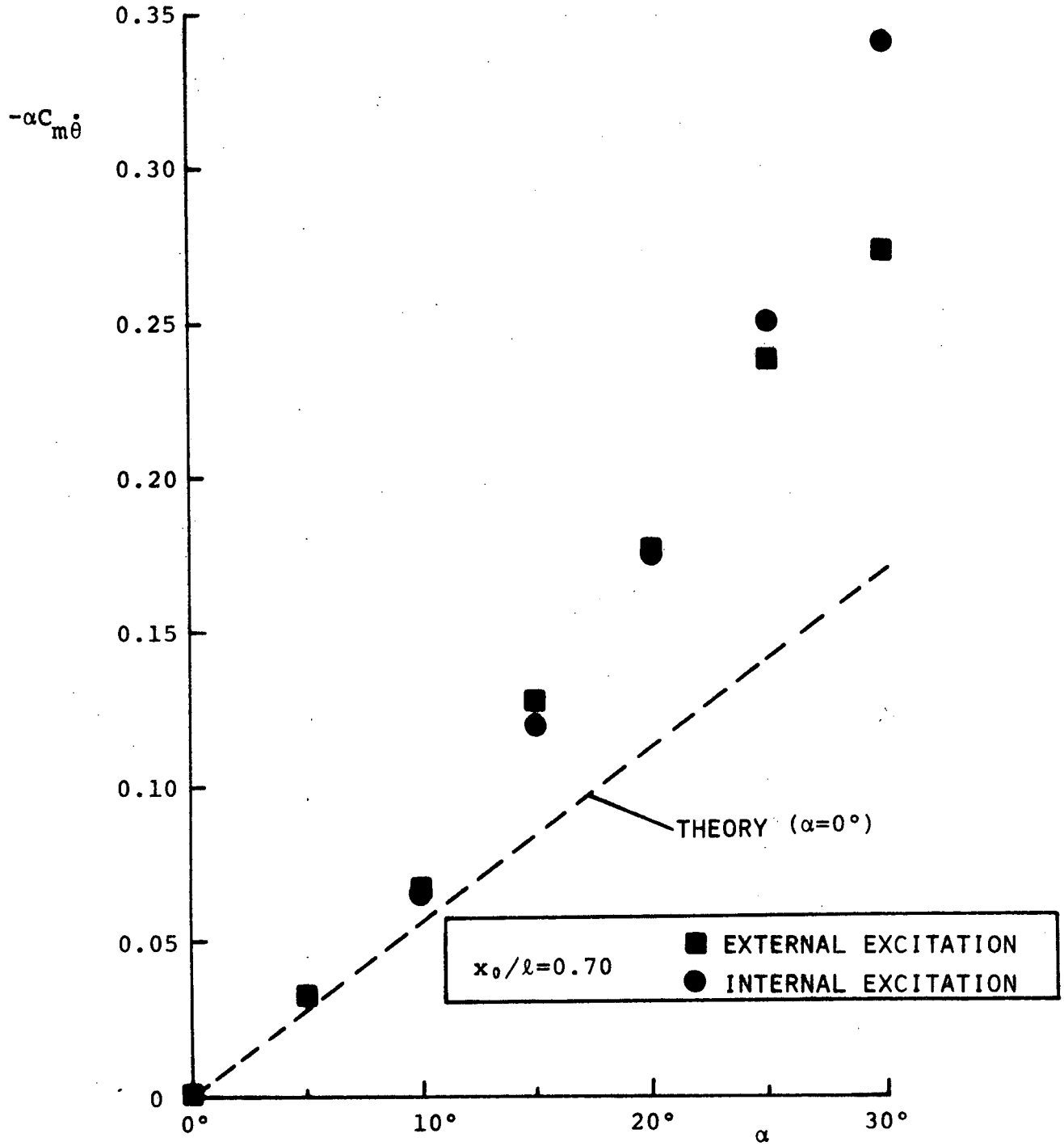

A) COMPARISON OF RESULTS OF THE TWO FULL-MODEL TECHNIQUES

FIG. 6 DAMPING FOR 7.75° CONE WITH B.L. TRIP REFERRED TO COMMON AXIS POSITION. (AXIS TRANSFER BASED ON ZERO INCIDENCE THEORY)

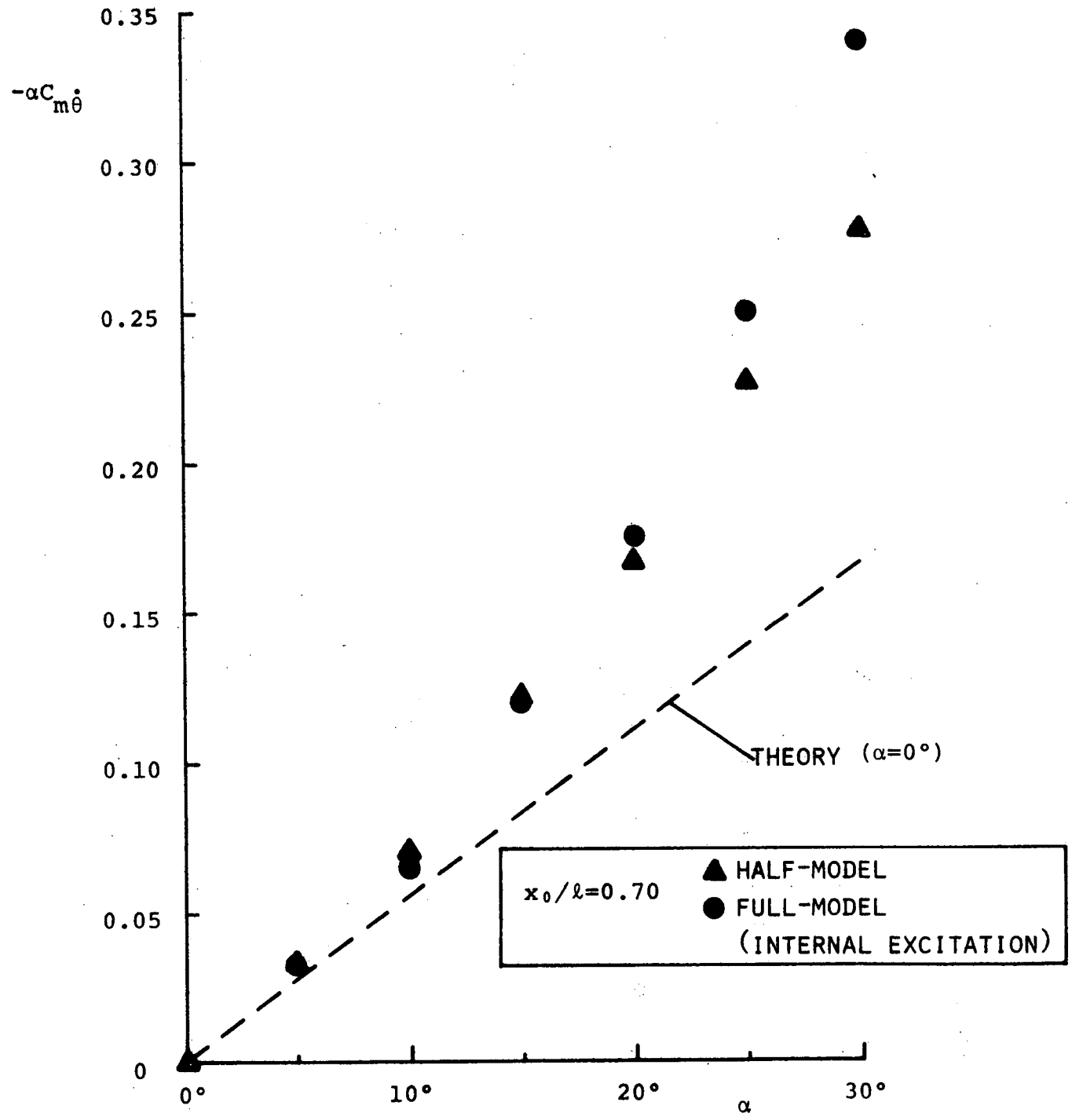

B) COMPARISON OF RESULTS OF THE HALF-MODEL AND THE FULL-MODEL (INTERNAL EXCITATION) TECHNIQUES

FIG. 6 CONCLUDED

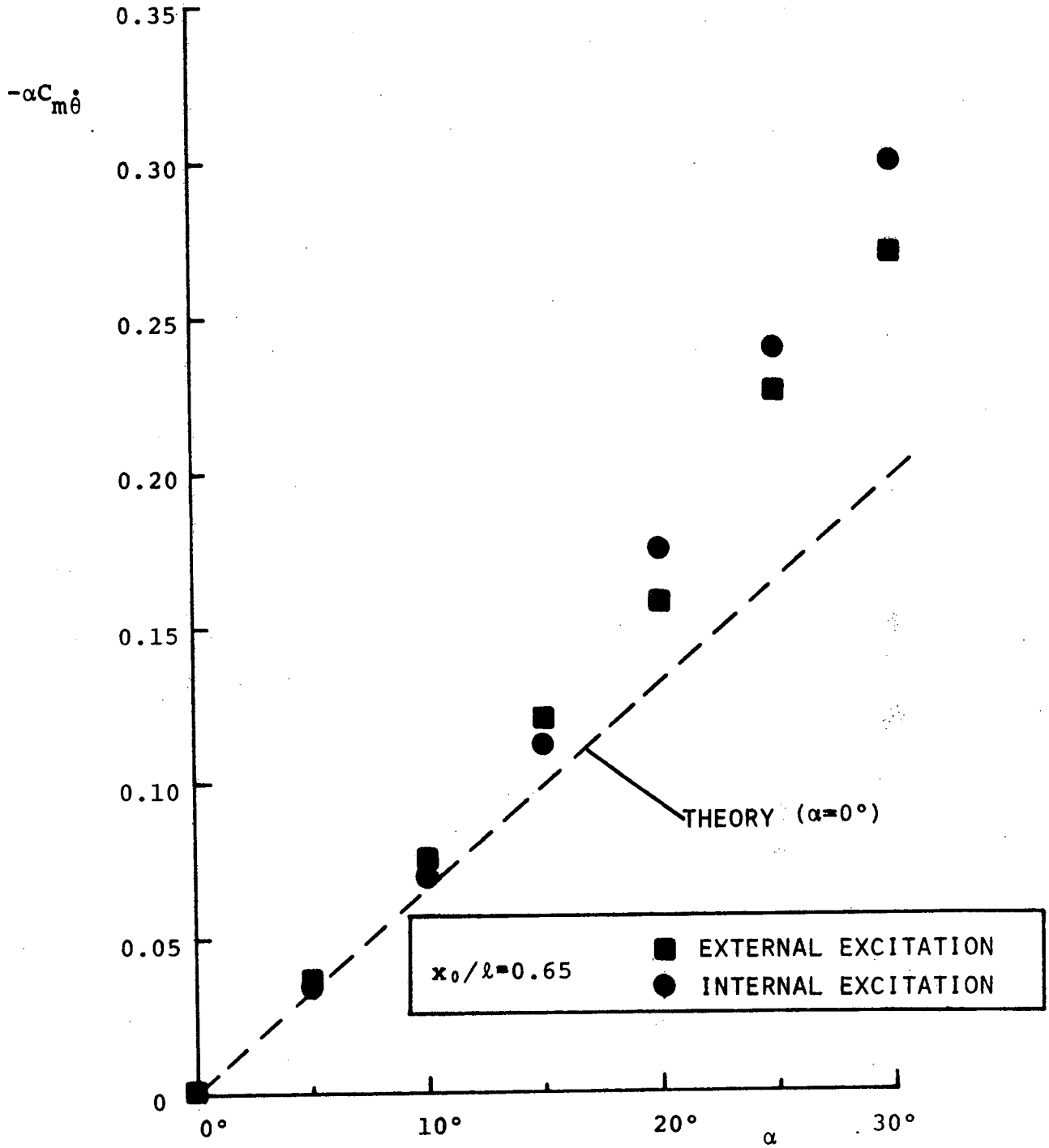

A) COMPARISON OF RESULTS OF THE TWO FULL-MODEL TECHNIQUES

FIG. 7 DAMPING FOR 10° CONE WITH B.L. TRIP REFERRED TO COMMON AXIS. (AXIS TRANSFER BASED ON ZERO INCIDENCE THEORY)

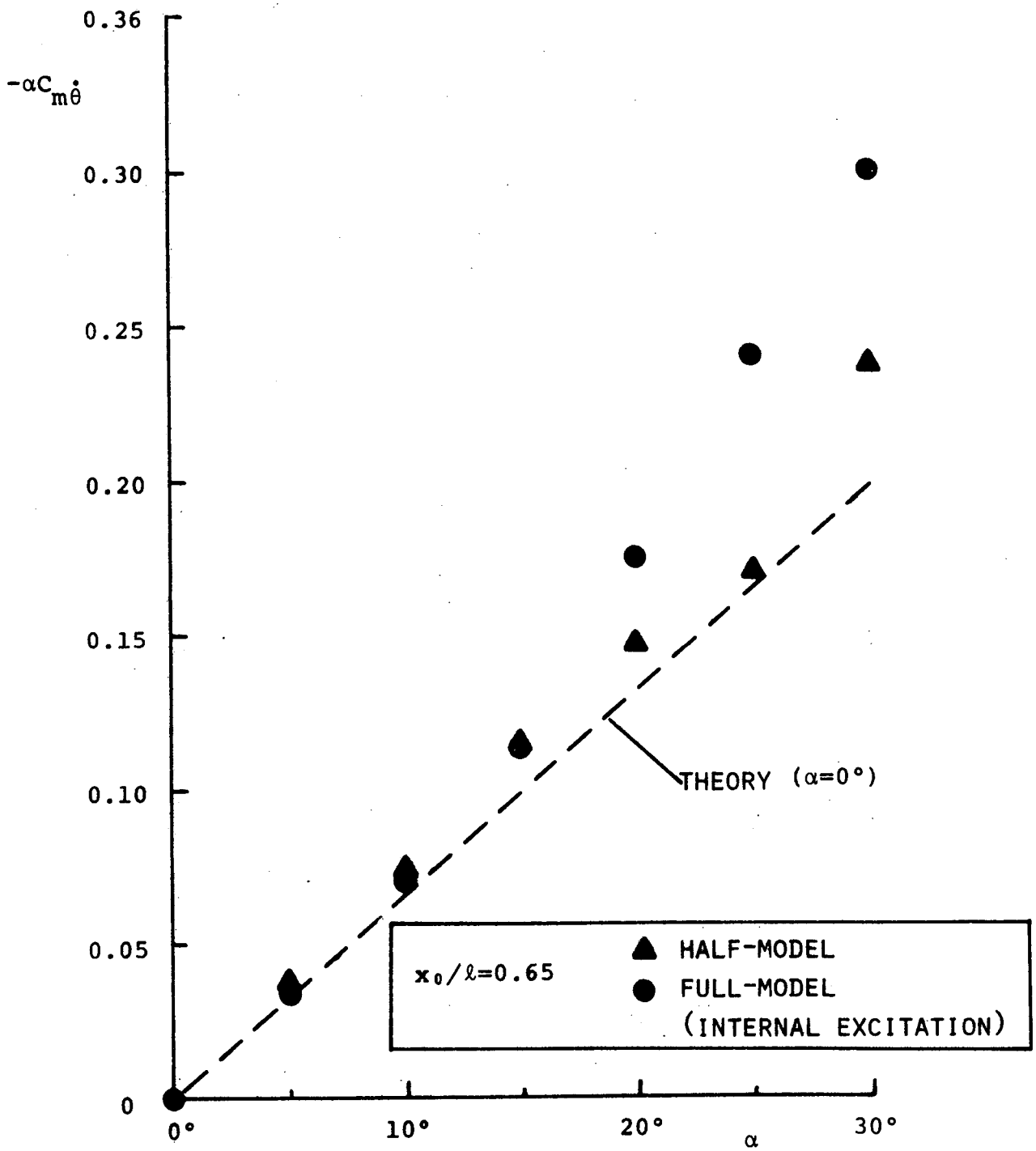

B) COMPARISON OF RESULTS OF THE HALF-MODEL AND THE FULL-MODEL (INTERNAL EXCITATION) TECHNIQUES

FIG. 7 CONCLUDED

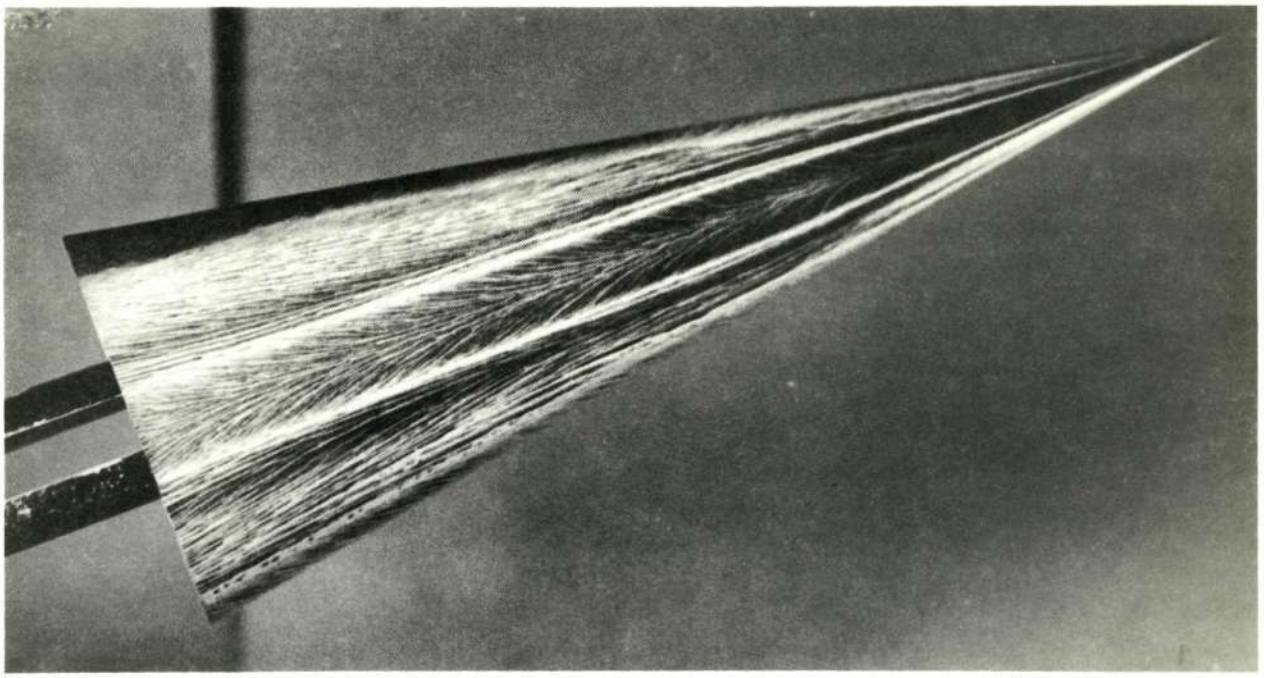

(MODEL AND STING ROTATED 90° FOR PHOTOGRAPH)

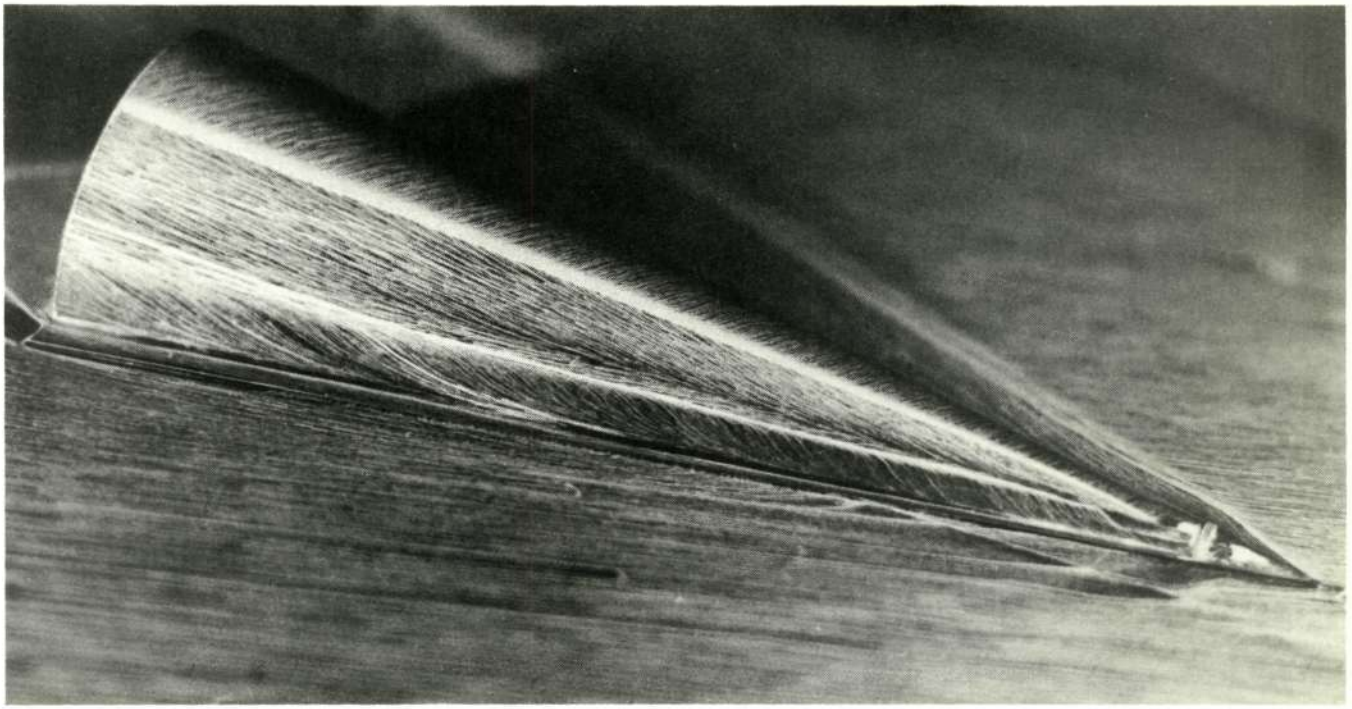

FIG. 8 OIL SURFACE-FLOW VISUALIZATION ON THE LEEWARD SIDE OF 10° CONE AT MACH 2 AND α=20°. FULL-MODEL (TOP) AND HALF-MODEL WITH B.L. TRIP (BOTTOM)